Article

Effect of dynamic PET scaling with LAI and aspect on the spatial performance of a distributed hydrologic model

Utku Demirci [1,*] and Mehmet Cüneyd Demirel [1]

[1] Department of Civil Engineering, Istanbul Technical University, İstanbul, 34467, Turkey; E-Mails: demirciu19@itu.edu.tr; demirelmc@itu.edu.tr

* Correspondence: demirciu19@itu.edu.tr; Tel.: +905065082266

Abstract: The spatial heterogeneity in hydrologic simulations is a key difference between lumped and distributed models. Not all distributed models benefit from pedo-transfer functions based on soil properties and crop-vegetation dynamics. Mostly coarse scale meteorological forcing is used to estimate water balance at the catchment outlet only. Mesoscale hydrologic model (mHM) is one of the rare models that incorporates remote sensing data i.e. leaf area index (LAI) and aspect to improve actual evapotranspiration (AET) simulations and water balance together. The user can select either LAI or aspect to scale PET. However, herein we introduced a new weighting parameter "alphax" that allows user to incorporate both LAI and aspect together for PET scaling. With this mHM code enhancement, the modeler has an also option of using raw PET with no scaling. In this study, streamflow, and AET are simulated using the mesoscale Hydrological Model (mHM) in Main (Germany) basin for the period of 2002-2014. The additional value of PET scaling with LAI and aspect for model performance is investigated using Moderate Resolution Imaging Spectroradiometer (MODIS) AET and LAI products. From 69 mHM parameters, 26 parameters are selected for calibration using Optimization Software Toolkit (OSTRICH). For calibration and evaluation, KGE metric is used for water balance and SPAEF metric is used for evaluating spatial patterns of AET. Our results show that AET performance of the mHM is highest when using both LAI and aspect indicating that LAI and aspect contain valuable spatial heterogeneity information from topography and canopy (e.g., forests, grasslands, and croplands) that should be preserved during modeling. The additional "alphax" parameter makes the model physically more flexible and robust as the model can decide the weights according to the study domain.

Keywords: cropland; evapotranspiration; LAI; aspect; remote sensing; mHM

1. Introduction

Hydrologic models are increasingly used to predict and control natural activities. To succeed in this, one relies on model calibration [1]. There are many parameters that affect rainfall-runoff models [2,3]. More parameters can be used, and more accurate results can be obtained with increasing computer processing power. The accuracy of one basin model is increased by the availability of large data sets and computation methods [4].

Various studies have assessed the importance of improving optimization procedures [5], choosing proper objective functions to appraise model performance [6], using probabilistic methods to take into account parameter uncertainty [7], calibrating the model to accommodate multiple targets [8], and selecting group of parameters which are part of step by step hydrologic process to meet various target [9,10]. Previous research [11] has established that LAI effect on AET. Much uncertainty still exists about the relationship between LAI and aspect.

Preprints (www.preprints.org) | NOT PEER-REVIEWED | Posted: 28 December 2022 doi:10.20944/preprints202212.0535.v1

Evapotranspiration plays a crucial role for water equilibrium and crop irrigation, drought estimation, and observation. In hydrological models, there are two types of evapotranspiration evaluation techniques. One estimates water surface evaporation, soil evaporation, and vegetable transpiration independently before integrating them to obtain basin evapotranspiration based on the land cover. The other one uses the Soil Moisture Extraction Function to first estimate potential evapotranspiration (PET) and then transform it into actual evapotranspiration (AET) [12]. We will focus on the second one, firstly, calculation of potential evapotranspiration.

There is a growing body of literature that recognizes physics-based hydrological models which have three types: fully distributed, semi-distributed and bulk model. In bulk models, only output data can be evaluated. However, in fully distributed models' results can be get from anywhere of basin and compare with satellite-based remote sensing data [11].

In this study, to compare AET which is obtained from MODIS (moderate resolution imaging spectrometer) with simulated values fully distributed the mesoscale Hydrological Model (mHM) is preferred.

To simulate AET, the mHM consider processes such as canopy interception, infiltration, surface runoff, base flow, deep percolation, flood routing, groundwater storage, snow-ice melting, and accumulation. Soil texture, digital elevation model, and land cover are physiographical data that were used to build model. Land cover data converted 3 layer (forest permeable, and impervious cover) [13].

For simulation of actual evapotranspiration 5 method is available with mHM. These are Penman-Monteith method [14], Priestley-Taylor method [15], Hargreaves-Sammani method, aspect driven and LAI driven method.[11,16] Previous research comparing LAI and aspect has found.[11,17,18] No previous study has investigated both LAI and aspect.

This paper examines scaling PET with both LAI and aspect and compare with it only LAI and only aspect driven cases All cases are tested in mHM spatial—pattern-oriented calibration of a catchment model in Main basin (Germany).

2. Materials and Methods

2.1. Study Area

The study area was selected as the Main. Main is the sub-basin of the Middle Rhine River. The Rhine is important for Europe in terms of water supply, irrigation, transportation, and industry. The Middle Rhine River consists of the Neckar, Moselle, and Main basins. The Main River formed from the Fichtel Mountains and the Red Main runs through Bamberg and then Würzburg. Mainz which is located 30 km west of Frankfurt joins The Rhine River.

The river was canalized in 1992 which connects the Rhine and Danube rivers and completes 3500 kilometers of the waterway from the North Sea to the Black Sea. Main-Danube Canal provides transportation between the North Sea and the Black Sea. The canal includes 16 locks and a hydroelectric power plant. These large engineering projects were done between 1960 and 1992. In the Rhine basin, mean annual precipitation varies from about 500 mm to 2000 mm (from the valley to the Alpine region). [19]

In this study, the area of the Main basin is 14117 km^2. The discharge value was taken from the outlet 6335500 which is in Würzburg. Annual discharge 243 mm. The annual precipitation is 736 mm, and the potential evapotranspiration is 773 mm. The melting of snow in the spring months causes high discharge values. The discharge increases between January and April and decreases between September and November. The reason for selecting the Main basin is that the gauge station has long-term discharge data without missing values. Location of Main basin in Germany, Leaf area index (LAI) in summer, elevation and gauge position in basin, river network and aspect driven from digital elevation model (DEM) of Main basin are shown in Figure 1.

Preprints (www.preprints.org) | NOT PEER-REVIEWED | Posted: 28 December 2022 doi:10.20944/preprints202212.0535.v1

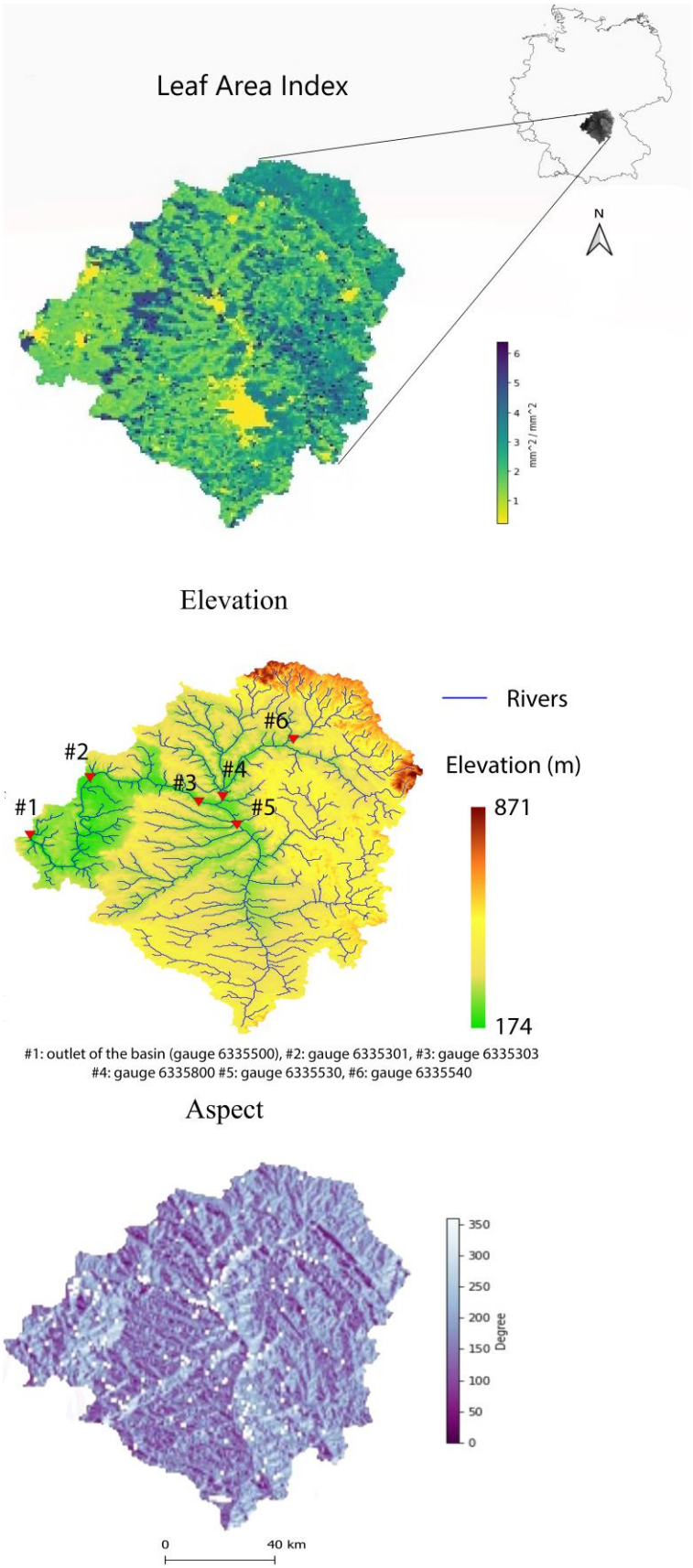

Figure 1 Physical charactersitics (LAI, DEM and aspect maps) of the study domain i.e. Main basin in Germany and streamflow gauge locations on the tributaries

Preprints (www.preprints.org) | NOT PEER-REVIEWED | Posted: 28 December 2022 doi:10.20944/preprints202212.0535.v1

2.2. AET (Actual Evapotranspiration)

Actual evapotranspiration is the second important process of water balance. About 60% of precipitation on land is transpired back into the air via evaporation and transpiration. Evaporations are water from soil, surface of water and canopy interception. Transpiration comes from plant leaves.

Despite the leaf area index, vegetation type is also an effective factor on AET. Evergreen forest contributes more annual AET than deciduous forest, but spatial analysis shows that expository parameters alter regionally. The driving variable of AET could be different for each basin [20].

Photosynthesis is an important factor on transpiration. Photosynthesis rate changes with illumination angle on leaves [21]. Therefore, aspect ratio effect transpiration and AET with leaf area index.

In mountainous basins, it is logical to use aspect ratio for AET correction, but the basin, which has low elevation difference, is found to be unpractical. By downscaling the referenced ET, the user may use the dynamic scaling algorithm that was proposed here to overlay pattern of LAI on the simulated AET patterns. The idea of a crop coefficient, which is used to transform reference ET into a potential amount of evapotranspiration (PET) for a specific vegetation that is different from the reference crop, like as the idea of a dynamic scaling function (DSF). DSF of LAI is shown equation at the below.

$$DSF = a + b(1 - e^{-c\,LAI}) \quad (1)$$

$$PET = DSF * ET_{ref} \quad (2)$$

a is the intercept term symbolize uniform scaling, b is the parameter symbolize vegetation dependence, c identify the rate of nonlinearity of LAI dependence [17].

2.3. mHM (mesoscale Hydrological Model)

mHM (mesoscale Hydrological Model developed by UFZ (Helmholtz Centre for Environmental Research). mHM is fully distributed, physically based, and continuous. The feature that distinguishes MHM from other hydrological models is that it is distributed with cells (grids). There are many different parameters are used for each cell in the workspace. With this feature, spatial analysis of the data used and the model run.

As the resolution of the basin increases, the variability of the characteristics of the basin in the computer environment can be well represented. Spatial variables of inputs and state variables are analyzed on their resolution in three different layers, at different scales: Level 0 (morphology), Level 1 (hydrology), and Level 2 (meteorology) as Figure 2.

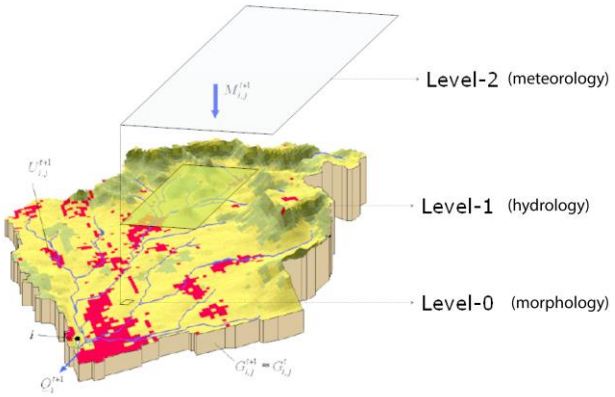

Figure 2 Spatial scales in model structure i.e. L0 is morphology, L1 is hydrology and L2 is coarse meteorologic forcing scale

 doi:10.20944/preprints202212.0535.v1

Level 0 is the most detailed scale of these layers. At this level, ground characteristics, morphological variables, land cover, and vegetation are processed. Spatial resolution processing is performed up to about 100 m at level 0 is done. Level 1 is the level where hydrological processes are processed. The process is performed at spatial resolutions between 1 km – 16 km. Finally, in Level 2, meteorological inputs and variables are processed. The resolution of level 2 is between 1 km and 25 km. Examination of the basins based on cells can reflect the heterogeneous nature of the land. Ordinary differential equations (ODE) were used to overcome the continuity problem, which is an examination of basin based on cells. Each cell with ODEs simulates the following processes: soil moisture dynamics, snow accumulation and melting, canopy interception, infiltration and surface runoff, evapotranspiration, subsurface storage and discharge generation, deep percolation and baseflow, and discharge attenuation and flood routing [22].

The execution of output-generating hydrological model routines occurs at a scale in between that of high-resolution watershed features and that of low-resolution meteorological forcing. Model parameters are regionalized by simple and built-in transfer functions that relate spatially scattered watershed properties to continuous parameter fields. With just a few calibration parameters, efficient model calibration is possible because to the control of transfer functions by global parameters. Additionally, it has been established that the mHM parameters are scale-independent, making it possible to calibrate the model at low spatial resolution and subsequently apply it at high spatial resolution using the same parameters. mHM has two transfer functions to increase the output of the geographically distributed model's realism even further. To consider for diverse land cover, it first couples completely dispersed vegetation features, namely the remotely sensed Leaf Area Index (LAI), to a spatially distributed crop coefficient. Second, it derives a field capacity based on a regionally variable root depth parameter using spatially distributed information on soil texture. For a spatial model-oriented calibration framework that seeks to improve the realism of spatially distributed model simulations, both transfer functions are crucial for the efficient integration of satellite-based measurements, such as evapotranspiration [23].

As a result of the ODEs analyzed for these processes, the hydrograph for each cell is obtained. The resulting hydrographs are between cells in Level 1.

The Muskingum method is used between cells and flow routing are obtained with this translation until the outlet. Instead of outlet flow, all cell flow can be seen in pattern [4].

2.4. Meterologic, morphologic and hydrologic data

Meteorology data taken from E-OBS (European observation) and MODIS (moderate resolution imaging spectroradiometer), morphology from SRTM (shuttle radar topography mission), ESD (European soil database) and HWSD (harmonized world soil database), hydrology from GRDC (global runoff data center). E-OBS is daily gridded dataset which observes daily precipitation sum, daily mean temperature, daily maximum temperature, and minimum temperature. Temperature and precipitation, is taken from E-OBS. Files are provided in netCDF-4 format and cover area is between 25N-71.5N x 25W-45E [24]. Leaf area index (LAI) and land cover data was received from MODIS dataset. The best image is selected by algorithm from sensors which are placed on NASA's Terra and Aqua satellites within 8-day periods [25,26]. DEM (digital elevation model) is received from SRTM (The Shuttle Radar Topography Mission). SRTM compare slightly different angles comes from two radar signals to calculate surface elevation. SRTM cover 80% of earth between 60N-56S [27]. Soil classes received from ESDB. ESDB is basic representation of soil classes on spatial pattern in Europe. The ESDB has 73 features of soil classes such as parent material, impermeable layer, restriction on agricultural use, soil water regime, altitude, slope, and physical, chemical, mechanical, and hydrological characteristics [28]. Soil classes information is also gotten from HWSD. HWSD is a worldwide combination of soil maps has more than 16000 soil attribute units. The raster

Preprints (www.preprints.org) | NOT PEER-REVIEWED | Posted: 28 December 2022 doi:10.20944/preprints202212.0535.v1

map of HWSD has 21600 rows and 43200 columns which have characterization such as organic Carbon, pH, soil depth, total exchangeable nutrients, gypsum and lime concentration, sodium exchange percentage, salinity, textural class, and granulometry [29]. Daily discharge values of 6 gauge (#6335500, #6335301, #6335303, #6335800, #6335530, #6335540) are received from GRDC. All inputs are summarized in Table 1.

Table 1 Description Morphologic and meteorologic inputs of mHM and their resolution and dataset resources[27,29–33]

Variable	Description	Resolution Degree	Source
Q (daily)	Streamflow	Point	GRDC
P (daily)	Precipitation	0.0625	EOBS
AET_{ref} (daily)	Actual evapotranspiration	0.0625	MODIS
PET_{ref} (daily)	Potential evapotranspiration	0.0625	E-OBS
T_{avg} (daily)	Average air temperature	0.0625	E-OBS
LAI	Fully distributed 12 monthly values based on an 8-day time-varying Leaf Area Index (LAI) dataset	0.001953125	MODIS
Land cover	Forest, pervious and urban	0.001953125	MODIS
DEM related data	Slope, aspect, flow accumulation, and direction	0.001953125	SRTM
Geology class	Two main geological formations	0.001953125	UFZ-Leipzig
Soil class	Fully distributed soil texture data	0.001953125	HWSD and ESD

2.5. Leaf Area Index (LAI) and Actual Evapotranspiration (AET)

Preprints (www.preprints.org) | NOT PEER-REVIEWED | Posted: 28 December 2022 doi:10.20944/preprints202212.0535.v1

MODIS global ET algorithm in NASA's earth observation system. It was developed for hydrological and ecological research using remote sensing data. During the calibration process of this study, the monthly MOD16 AET was used. LAI was used. ET data was obtained from the MOD15 algorithm at 8-day, monthly, and yearly intervals. Available in 1 km spatial resolution. MODIS LAI product as a long-term monthly average was inserted into the model. LAI maps plant growth on low-resolution PET data. It is used to introduce the dynamics of PET and directly affects the results of AET [11]. Leaf Area Index (LAI) is taken into consideration at the L0 level and up-scaling from L0 to the L1 level. LAI is calculated as in equation below [34]:

$$Leaf\ area\ per\ plant = Leaf\ area\ per\ plant\ x\ Number\ of\ plants\ per\ unit\ area \quad (3)$$

2.6. Aspect and Actual Evapotransporation (AET)

Aspect is a Digital Elevation Model (DEM) related data. Aspect is a very effective parameter for snow distribution with slope, elevation, and insolation [35]. The LAI is considered with aspect to obtain more accurate prediction of evapotranspiration in both mountain and low elevation variety basins.

The original scaling factor in mHM is based on an aspect-driven term and a lumped minimum correction. In mountainous areas, considering aspect ratio for AET correction is very logical; but, this is found to be irrelevant for basin which has a low elevation difference [17].

2.7. Objective Functions

2.7.1. Kling-Gupta (KGE)

KGE takes values equal or smaller than 1.

$$KGE=1-ED \quad (4)$$

$$ED=\sqrt{(1-r)^2+(1-\alpha)^2+(1-\beta)^2} \quad (5)$$

" r" is the Pearson correlation coefficient. " α" is the ratio between the average of the forecast values and the average of the observed values. "β" is the ratio between standard deviation of forecast values and standard deviation of observation [36]. 1-KGE=ED=0 is the objective function.

2.7.2. Spatial Efficiency Metric (SPAEF)

In this case aspect driven results have been checked. SPAEF metric consist of correlation, coefficient of variation and histogram match. These components help to overcome sophisticated hydraulic models [37].

$$SPAEF=1-\sqrt{(\alpha-1)^2+(\beta-1)^2+(\gamma-1)^2} \quad (6)$$

$$\alpha=\rho(obs,sim),\ \beta=\left(\frac{\sigma_s}{\mu_s}\right)/\left(\frac{\sigma_o}{\mu_o}\right),\ \gamma=\frac{\sum_{j=1}^{n}\min(K_j,L_j)}{\sum_{j=1}^{n}K_j} \quad (7)$$

"α" is the Pearson correlation coefficient which show correlation between observed and simulated values. "β" symbolizes spatial variability which is the fraction of the coefficient of variation. "ɣ "stands for histogram intersection, K refers to observed pattern, and L refers to simulated pattern.

2.8. Model Calibration and Validation

Preprints (www.preprints.org) | NOT PEER-REVIEWED | Posted: 28 December 2022 doi:10.20944/preprints202212.0535.v1

For 5 different cases sensitive parameters are calibrated with 750 iterations by OSTRICH (Optimization Software Toolkit). There is more than one objective function, therefore, the PADDS (Pareto Archived Dynamically Dimensioned Search) algorithm is preferred. Pareto-front select non-dominated runs in 750 runs. Non-dominated runs provide choice to user between objective functions to select a parameter set and group for next model application. Non-dominated runs maintain improvement on both objective functions simultaneously. The PADDS produces components randomly in the distribution of runs along the pareto front. The tradeoff between the spatial ET performance and the temporal discharge performance is clearly shown in all cases as a pareto front. The SPAEF residuals for the normalized the simulated patterns after normalization are more different to the normalized target pattern than the original ET patterns. However, the performance of the water balance is comparable between cases [23]. Scheme of calibration for cases are shown in Figure 3.

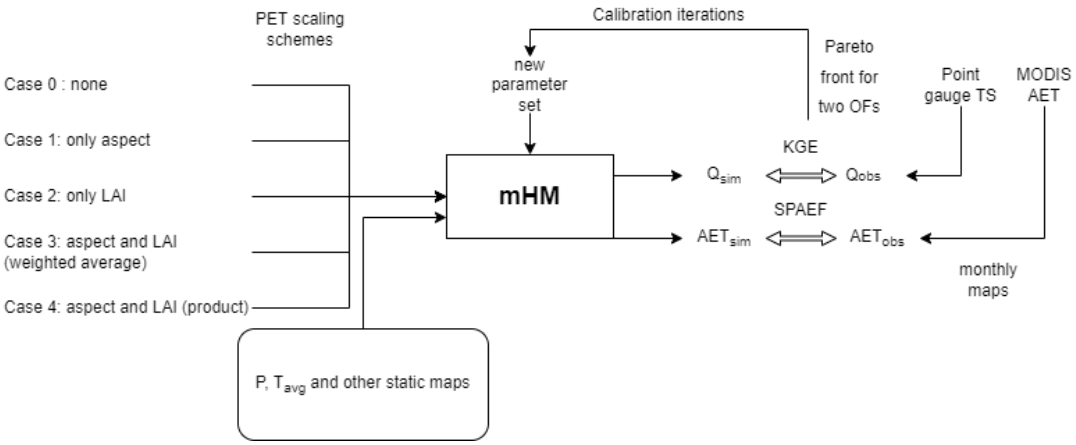

Figure 3. Calibration scheme

OSTRICH minimizes objective function of KGE and SPAEF. Optimal value for KGE and SPAEF is 1. Square residual defined for SPAEF for spatial pattern of AET (8) and sum of 6-gauge square residual defined for KGE (9).

$$SR_{AET}=(1-SPAEF)^2 \tag{8}$$

$$SSR_Q=\sum_i^6 (1-KGE_i)^2 \tag{9}$$

MODIS AET values are monthly maps between 2002 and 2014. These maps were added to the model taking quarterly terms as March-April-May (MAM), June-July-August (JJA), and September-October-November (SON). End of the iteration best parameter sets selected for every case and run once more to validate results. Best parameter sets selected smallest value of sum of objective function of KGE and SPAEF. To validate results best parameter run again then SPAEF and KGE values are checked [38].

Case 0, PET correction driven by neither LAI nor aspect. The purpose of adding this case to see the vegetation and aspect effect by comparing other cases. Case 1, aspect driven results have been checked. Aspect defines direction of slope faces. Aspect is a degree that takes values from 0 to 360. Case 2, LAI driven results have been checked. LAI is the ratio between the vegetation area and the total area. Therefore, LAI is a unitless parameter.

Preprints (www.preprints.org) | NOT PEER-REVIEWED | Posted: 28 December 2022 doi:10.20944/preprints202212.0535.v1

Case 3, the LAI, and aspect driven by the weight number results have been checked. LAI and aspect driven by the weight parameter between LAI and aspect. The weight parameter between LAI and aspect is a number between 0 and 1. LAI multiplied by weight parameter and aspect multiplied by (1- weight parameter) and summed for AET correction. PET correction method added mHM source file like in Equation 10 [39].

$$pet = pet\_in(k) * ((petLAIcorFactorL1(k) * alphax) + (fAsp(k) * (1 - alphax))) \quad (10)$$

Case 4; the LAI, and aspect correction numbers are multiplied for PET correction and the results have been checked. This case added to search effect of aspect on photosynthesis and effect of both on actual evapotranspiration. Equation 11 is added to methods of mHM [39].

$$pet = pet\_in(k) * petLAIcorFactorL1(k) * fAsp(k) \quad (11)$$

3. Results

3.1. Model Sensitivity Analysis

Hydrological modeling is necessary for most determinations about managing resources quantitatively. The functions of a natural system are often represented by highly parameterized, physically justified, process-based numerical models. This allows the models to be used to assess the effectiveness of management tactics or the system's response to environmental changes [40].

All morphological and meteorological data transform to appropriate resolution and time scale. Instead of using all 69 parameters of mHM, most sensitive 26 parameter used for this study. Considering all parameters may cause time consumption therefore, sensitivity analysis based on AET, and discharge was calculated with PEST [40] (Model-Independent Parameter Estimation and Uncertainty Analysis) by objective function of SPAEF and KGE metrics. Objective functions are SPAEF for the spatial pattern of actual evapotranspiration, and KGE for 6 discharge gauges.

26 most sensitive parameters are shown in Figure 4. These parameters selected based on the combined sensitivity of KGE and SPAEF. Based on KGE most sensitive 10 parameters controlling water balance are rotfrcofclay, rotfrcoffore, pet_apervi, ptflowconst, ptfksconst, infshapef, ptflowdb, alphax, pet_bb, mincorfacpet. The other bjective function SPAEF is most sensitive to the parameters rofrcofclay, orgmatimper, rotfrcoffore, pet_apervi, slwintreceks, rotfrcofimp, pet_aimpervi, alphax, pet_bb, infshapef, which has some similar parameters with KGE also has more PET parameters. Soil properties effect on SPAEF is remarkable result.

All sensitive parameters normalized between 0 and 1. Description and range of parameter are shown in Table 2. As shown in Figure 4 weight parameter between LAI and aspect (alphax) is eight most sensitive parameter not only for KGE for gauges but also for SPAEF for actual evapotranspiration.

Preprints (www.preprints.org) | NOT PEER-REVIEWED | Posted: 28 December 2022 doi:10.20944/preprints202212.0535.v1

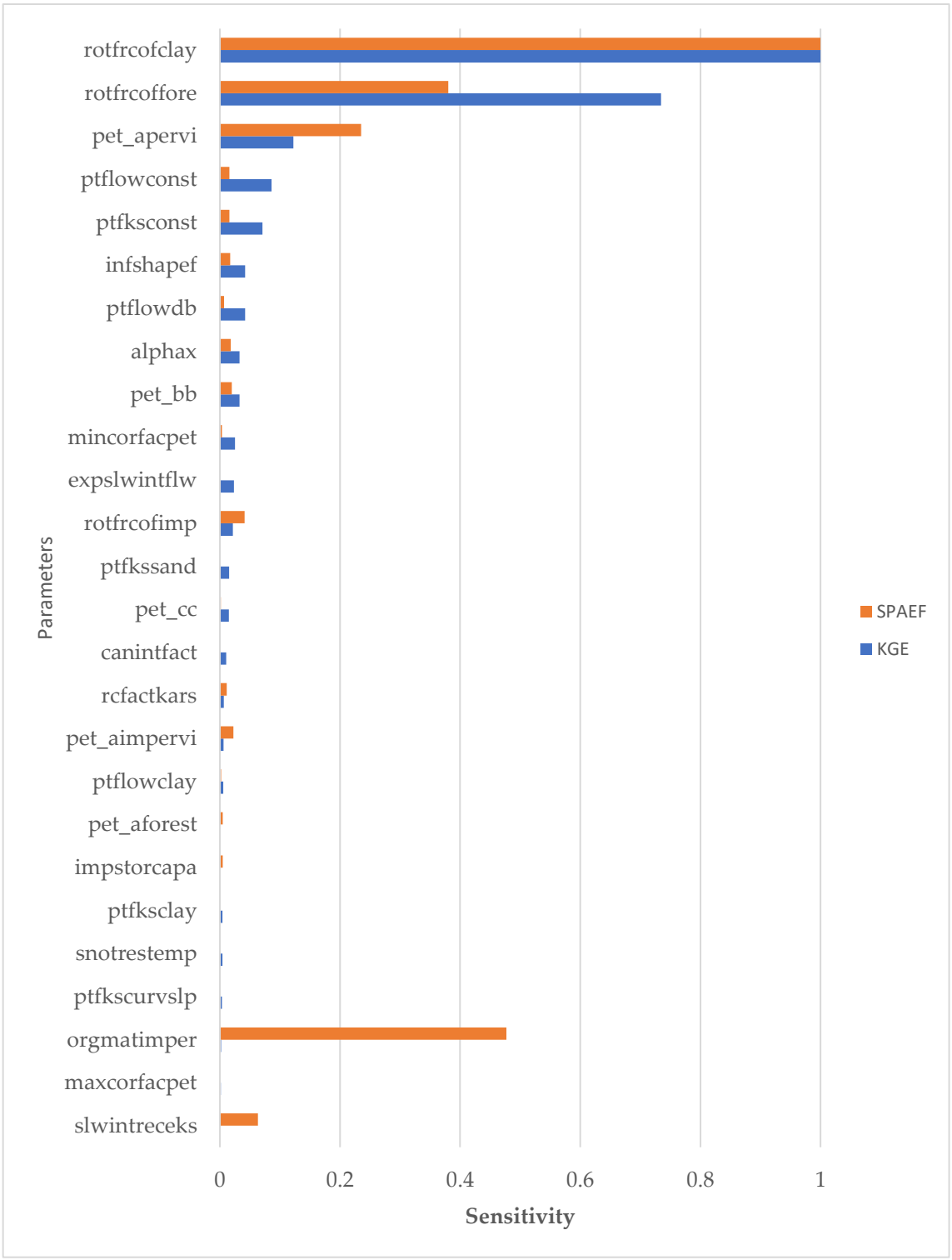

Figure 4. Most Sensitive 26 Parameters according to objective function of SPAEF and KGE. Sensitivity calculated by PEST.

Preprints (www.preprints.org) | NOT PEER-REVIEWED | Posted: 28 December 2022 doi:10.20944/preprints202212.0535.v1

Table 2 Description of 26 selected sensitive parameters and their range in mHM

Parameter Name	Description	Min	Max
rotfrcofclay	root fraction coefficient clay	0.9	0.999
rotfrcoffore	root fraction coefficient forest	0.9	0.999
pet_apervi	PET scaling: pervious	-0.3	1.3
ptflowconst	PTF saturated water content: constant	0.6462	0.9506
ptfksconst	PTF hydraulic conductivity: constant	-1.5	-1.2
infshapef	Infiltration shape factor	1	4
ptflowdb	PTF saturated water content: coefficient bulk density	-0.3727	-0.1871
alphax	Weight parameter between LAI and aspect	0	1
pet_bb	PET scaling: range	0	1.5
mincorfacpet	minimum correction factor of PET	0.7	1.3
orgmatimper	Organic matter content for impervious zone	0	1
rotfrcofimp	Root fraction coefficient impervious	0.9	0.999
ptfkssand	PTF hydraulic conductivity: Sand	0.0042	0.01
pet_cc	PET scaling: shape	-2	0
canintfact	Canopy interception factor	0.15	0.4
rcfactkars	Recharge factor karstic	-5	5
pet_aimpervi	PET scaling: impervious	0.3	1.3
ptflowclay	PTF saturated water content: clay	0.0001	0.0029
ptfksclay	PTF hydraulic conductivity: clay	0.003	0.0129
snotrestemp	Snow temperature threshold for rain and snow separation	-2	2
ptfkscurvslp	PTF hydraulic conductivity: curve slope	51	56
slwintreceks	Slow interception	1	30
impstorcapa	Impervious storage capacity	0	5
pet_aforest	PET scaling: forest	0.3	1.3
aspectreshpet	Aspect threshold PET	160	200
maxcorfacpet	Maximum correction factor of PET	0	0.2

3.2. Spatial Pattern Result of AET

In Germany, Main basin is modeled by fully distributed hydrologic model mHM. For two objective functions (KGE and SPAEF), the best-balanced solution is chosen for visualization. SPAEF value for AET and KGE value for outlet discharge are calculated with three-month period for evaluated cases. Three-month periods are MAM (March, April, and May), JJA (June, July, and August), and SON (September, October, and November).

The results are according to the best case in non-dominated solutions. If there is no other better solution in two objective functions is called non-dominated. All cases compared with MODIS AET data in Figure 5. Best non-dominated solution (minimum summation of KGE and SPAEF) nearest to origin selected to visualize.

Preprints (www.preprints.org) | NOT PEER-REVIEWED | Posted: 28 December 2022 doi:10.20944/preprints202212.0535.v1

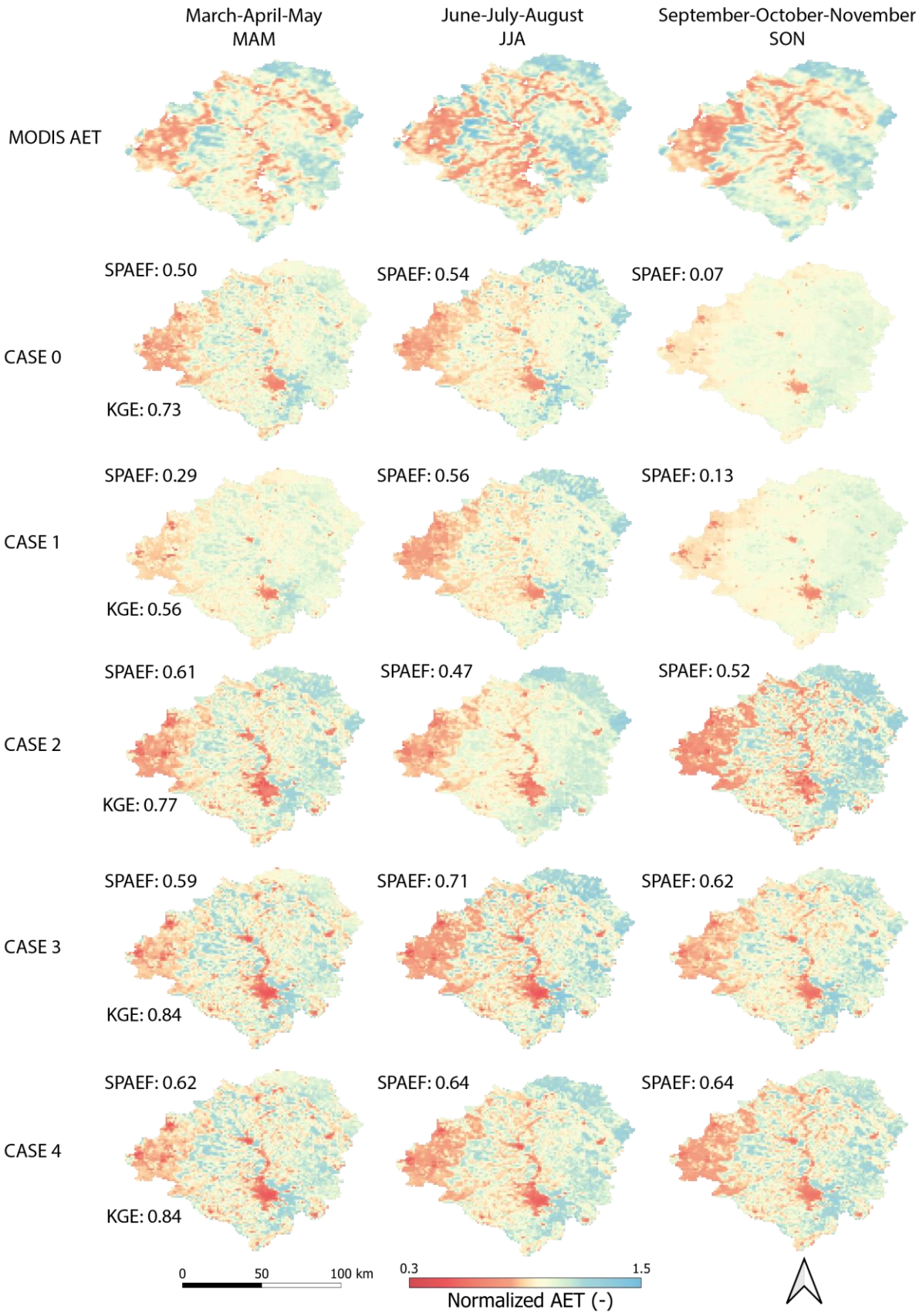

Figure 5. Spatial pattern results of average 3-month periods compared with observed MODIS AET

Preprints (www.preprints.org) | NOT PEER-REVIEWED | Posted: 28 December 2022 doi:10.20944/preprints202212.0535.v1

According to result (Figure 5), ignoring aspect and LAI for AET in case 0 cause the worst result in three terms (SPAEFs are 0.50, 0.54 and 0.07). KGE is 0.73. KGE of base case performs better than case 1. Spatial pattern performances are also not too bad based on JJA and MAM because there are more sensitive parameters than LAI and aspect. Therefore, we did not expect it to be irrelevant to observed MODIS AET, even it is driven neither LAI nor aspect.

According to the result (Figure 5) of Case 1 (aspect driven), the aspect correction improves the AET performance. Three-term SPAEF results are 0.29, 0.56 and 0.13). KGE result is 0.56. Case 1 spatial pattern results are slightly better than case 0. For snow-dominated mountain basin, aspect-driven case may give better result than this.

According to result (Figure 5) of Case 2 (LAI driven), gives much better performance than Case 0 and Case 1. LAI effect is more significant than aspect in Main basin. Three-term SPAEF results are 0.61, 0.47 and 0.52). KGE result is 0.77. Case 2 result is much better than case 0 and case 1. This result is very similar to previous studies [11,17].

Case 3 performance better than other cases. Three-term SPAEF results are 0.59, 0.71 and 0.62. KGE result is 0.84 is much better than other cases. Weight parameter helped better constrain the model parameters connected to actual evapotranspiration when compared to cases based on only LAI and only aspect.

Case 4 is also show good results like Case 3. SPAEF values for spatial pattern of AET are 0.56, 0.62 and 0.64. KGE is 0.64. LAI driven correction parameter multiplied with aspect and PET. "alphax"parameter is not used in this case. This shows that without adding new parameter, just influencing LAI and aspect to model enough to get much better result. The spatial pattern of Case 3 and Case 4 spatial pattern and water balance performance are very close.

3.3. Water Balance result of gauges

Simulated KGE result according to observed discharges are shown in Table 3. Validations are run also with 6 gauges. Case 3 and case 4 show better KGE performance in most of gauges. Location of gauges are shown in Figure 1. Based on these gauges, KGE discharge result compared to observed data is shown in Table 3. Improved performance of case 3 and case 4 are also can be seen in most of the gauges. The most surprising aspect of the data is that water balance score of case 3 is better than case 4. Instead of single outlet gauge validation, case 3 is more compatible for multigauge calibration than case 4.

Table 3. Model validation gauges from internal tributaries of the Main basin

	KGE				
Gauges	**CASE 0**	**CASE 1**	**CASE 2**	**CASE 3**	**CASE 4**
6335500	0.14	0.3	0.07	0.55	0.30
6335301	0.13	0.28	0.04	0.54	0.28
6335303	-0.03	0.21	-0.24	0.48	0.07
6335530	-0.67	-0.03	-0.85	-0.01	-0.46
6335800	0.57	0.53	0.45	0.67	0.52
6335540	-4.38	-3.49	-4.62	-4.07	-4.94

3.4. Non-Dominated Result and best parameter of cases

Preprints (www.preprints.org) | NOT PEER-REVIEWED | Posted: 28 December 2022 doi:10.20944/preprints202212.0535.v1

After 750 iterations, selected non-dominated solutions and marked best cases are represented in Figure 6.

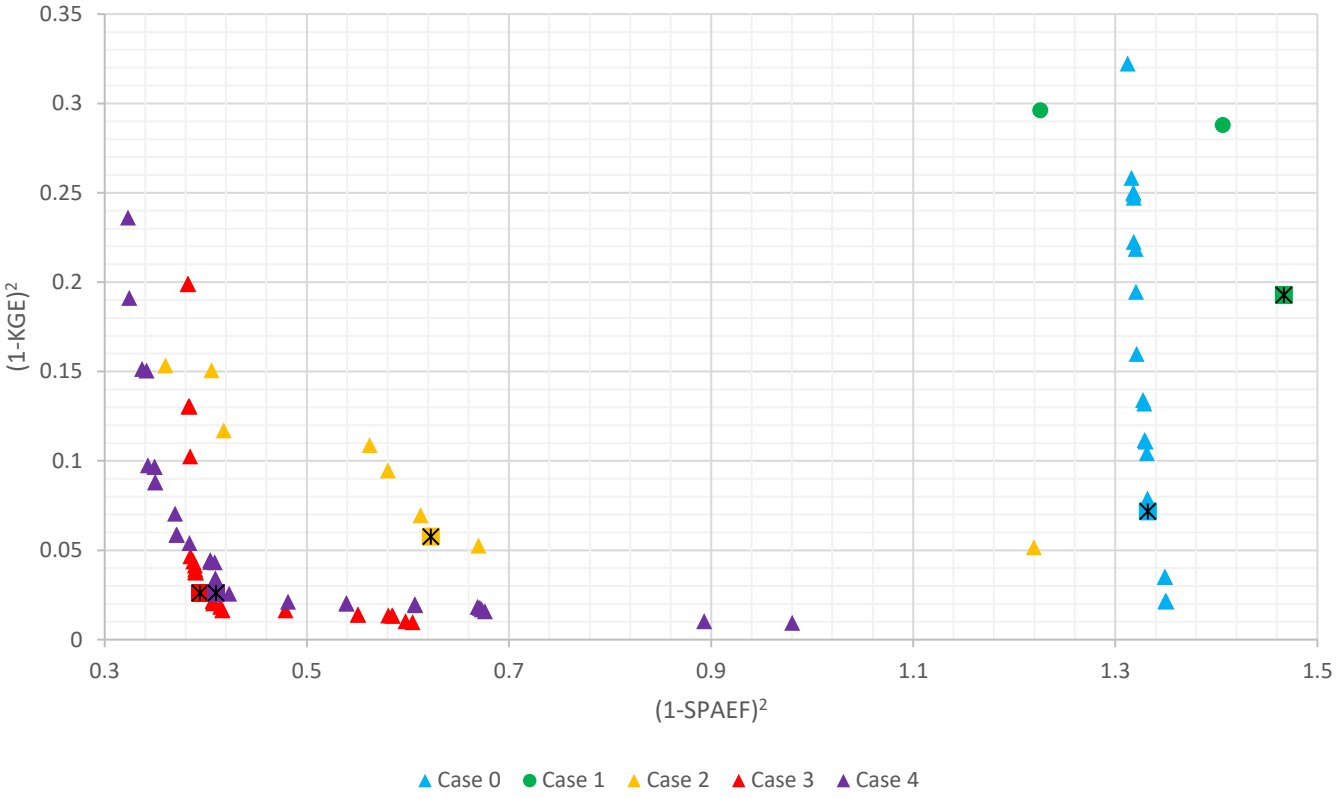

Figure 6. Non-dominated results of cases compared with OSTRICH and best result of each cases marked

Objective function of KGE and SPAEF are shown in axis. Closest point of each cases marked as best parameter set of those cases. Case 0 (blue) and case 1 (green) has very poor SPAEF performance and poor KGE performance as expected. Increased performance with LAI is also clearly visible on case 2 (yellow). Performance of Case 3 and case 4 are better than all other cases. Best result of case 3 is slightly better than case 4. However, spatial pattern score of case 4 is better in many calculations. On the contrary, streamflow score of case 3 is better in some of the calculations. Taken together, these results suggest that there is an association between LAI and aspect to calibrate hydrologic model.

4. Discussion

Hydrological models are widely used across the world due to the requirement to forecast how changes in the climate and in land use would affect the discharge regime, particularly given their capacity to forecast flows in both metered and unmetered watersheds. These estimators do, however, carry some risk because of model bias, inaccurate input data, and inaccurate model parameter values. Decisions concerning hydrological fluxes are based on model results, which hydrological modelers use to affect impulses. Numerous research has examined and estimated a range of input data that reflect those in conceptual and physically distributed models to better understand the various ways that models work [1,3,4,11,12,17,18,41].

Models like mHM are distributed spatially and comprise equations with one or more region coordinates for simulating the volume of discharges and bulk storage as well as the spatial production of hydrological variables across a basin. These types of models are inherent to their design and operation and place heavy demands on both computing time and data specifics. The outcomes of this study show how the geograph-

 doi:10.20944/preprints202212.0535.v1

ical model responds to the operational characteristics of the input data depending on the research aim.

The present study was designed to determine the effect of LAI and aspect on hydrologic models. For this purpose, cases labeled as case 0 to case 4 with different input and varying equation. Case 0 configured without LAI and aspect correction. Case 1 is designed with aspect and Case 2 with LAI only. In Case 3 coefficient added to LAI and aspect correction and summed. Case 4 is built by multiplying LAI and aspect correction which makes it possible to observe model performance without adding parameter.

The most obvious finding that the emerges from the analysis is that simulation performs better when LAI and aspect are used together. Spatial pattern of AET of case 2 is much more similar than case 0 and case 1. This result seem to be consistent with other research which found in [11,18]. It seems possible that these results are due to properties of Main basin. Snow dominated, rain dominated or basins which have different type vegetation may differ rate of effect between aspect and LAI. However, in any case, both LAI and aspect effect will be important.

Our next research will be about to run case 3 and case 4 in different type of basin. For example, mountainous areas, snow dominated areas or in basin which have different climate type.

5. Conclusion

The main goal of this study is to assess the effect of LAI and aspect together on the model simulated AET and water balance. For this purpose, 5 cases (experiments) are designed for the Main basin (Germany) with fully distributed hydrologic model mHM. Firstly, source code of mHM is modified and added a new parameter i.e. alphax. Then, sensitive parameters are determined for calibration. For each case, discharge calibrated with KGE metric by comparing with measured outlet discharge, and spatial pattern of AET calibrated with objective function of SPAEF by comparing with MODIS AET monthly data. The following conclusions are drawn based on the calibration and validation results:

- Using unscaled PET is sufficient for a reasonable water balance like in lumped models.
- Using only aspect for PET scaling deteriorates water balance performance and not improves the AET performance.
- Using only 12 monthly LAI maps for dynamic PET scaling significantly improves AET and water balance performance of the mHM.
- The product of LAI and aspect without weighting also improves the AET and water balance performance of mHM.
- The weighting LAI and aspect using alphax parameter reveals slightly better performance than the product of LAI and aspect.

Further research should explore the added value of daily LAI maps instead of monthly maps on dynamic PET correction.

Author Contributions: For research articles with several authors, a short paragraph specifying their individual contributions must be provided. The following statements should be used "Conceptualization, U.D. and M.C.D.; methodology, U.D.; software, U.D.; validation, U.D. and M.C.D.; formal analysis, U.D.; investigation, U.D.; resources, U.D.; data curation, U.D.; writing—original draft preparation, U.D.; writing—review and editing, U.D. and M.C.D.; visualization, U.D.; supervision, M.C.D.; project administration, M.C.D. All authors have read and agreed to the published version of the manuscript." All authors have read and agreed to the published version of the manuscript.

Data Availability Statement: Data, scripts and model setups will be made available and shared upon request to the corresponding author. The Fortran source code of the mHM v5.11.1_r is publicly available from an online repository; https://doi.org/10.5281/zenodo.7483954

Acknowledgments: We acknowledge the financial support by Turkish Scientific and Technical Research Council (TUBITAK) grant number 118C020 and the National Center for High-Performance Computing of Turkey (UHeM) under grant number 1007292019.

Conflicts of Interest: The authors declare no conflict of interest.

References

1. Zhang, X.; Srinivasan, R.; Zhao, K.; Liew, M. Van Evaluation of Global Optimization Algorithms for Parameter Calibration of a Computationally Intensive Hydrologic Model. *Hydrol. Process.* **2009**, *23*, 430–441, doi:10.1002/hyp.7152.

2. Li, J.; Chen, H.; Xu, C.-Y.; Li, L.; Zhao, H.; Huo, R.; Chen, J. Joint Effects of the DEM Resolution and the Computational Cell Size on the Routing Methods in Hydrological Modelling. *Water* **2022**, *14*, 797, doi:10.3390/w14050797.

3. Gong, L.; Widén-Nilsson, E.; Halldin, S.; Xu, C.-Y. Large-Scale Runoff Routing with an Aggregated Network-Response Function. *J. Hydrol.* **2009**, *368*, 237–250, doi:10.1016/j.jhydrol.2009.02.007.

4. ALP, H.; DEMİREL, M.C. *Hydrological Model Structure and Calibration Algorithm Effect on Discharge Simulation Performance*; 2022;

5. Wang, Q.J. The Genetic Algorithm and Its Application to Calibrating Conceptual Rainfall-Runoff Models. *Water Resour. Res.* **1991**, *27*, 2467–2471, doi:10.1029/91WR01305.

6. Dawdy, D.R.; O'Donnell, T. Mathematical Models of Catchment Behavior. *J. Hydraul. Div.* **1965**, *91*, 123–137, doi:10.1061/JYCEAJ.0001271.

7. Kuczera, G. On the Validity of First-Order Prediction Limits for Conceptual Hydrologic Models. *J. Hydrol.* **1988**, *103*, 229–247, doi:10.1016/0022-1694(88)90136-9.

8. Gupta, H.V.; Sorooshian, S.; Yapo, P.O. Toward Improved Calibration of Hydrologic Models: Multiple and Noncommensurable Measures of Information. *Water Resour. Res.* **1998**, *34*, 751–763, doi:10.1029/97WR03495.

9. Harlin, J. Development of a Process Oriented Calibration Scheme for the HBV Hydrological Model. *Hydrol. Res.* **1991**, *22*, 15–36, doi:10.2166/nh.1991.0002.

10. Shamir, E.; Imam, B.; Gupta, H. V.; Sorooshian, S. Application of Temporal Streamflow Descriptors in Hydrologic Model Parameter Estimation. *Water Resour. Res.* **2005**, *41*, doi:10.1029/2004WR003409.

11. AVCUOGLU, M.B.; DEMİREL, M.C. On the Utility of Remotely Sensed Actual ET and LAI in Hydrologic Model Calibration. *Tek. Dergi* **2022**, doi:10.18400/tekderg.1067466.

12. Zhao, L.; Xia, J.; Xu, C.; Wang, Z.; Sobkowiak, L.; Long, C. Evapotranspiration Estimation Methods in Hydrological Models. *J. Geogr. Sci.* **2013**, *23*, 359–369, doi:10.1007/s11442-013-1015-9.

13. Rakovec, O.; Kumar, R.; Mai, J.; Cuntz, M.; Thober, S.; Zink, M.; Attinger, S.; Schäfer, D.; Schrön, M.; Samaniego, L. Multiscale and Multivariate Evaluation of Water Fluxes and States over European River Basins. *J. Hydrometeorol.* **2016**, *17*, 287–307, doi:10.1175/JHM-D-15-0054.1.

14. Monteith, J.L. EVAPORATION AND ENVIRONMENT. *Symp. Soc. Exp. Biol.* **1965**, *19*, 205–234.

15. Jensen, M.; Burman, R.; Allen, R. Evapotranspiration and Irrigation Water Requirement. *ASCE Am. Soc. Civ. Eng.* **1990**, *131*.

16. Samaniego, Brenner, J., Craven, J., Cuntz, M., Dalmasso, G., Demirel, M. C., Jing, M.; 803 Kaluza, M., Kumar, R., Langenberg, B., Mai, J., Müller, S., Musuuza, J., Prykhodko, V.; 804 Rakovec, O., Schäfer, D., Schneider, C., Schrön, M., Schüler, L., … Attinger, S. The Mesoscale Hydrologic Model - MHM v5.11.1 (v5.11.0). **2021**.

17. Demirel, M.C.; Mai, J.; Mendiguren, G.; Koch, J.; Samaniego, L.; Stisen, S. Combining Satellite Data and Appropriate Objective Functions for Improved Spatial Pattern Performance of a Distributed Hydrologic Model. *Hydrol. Earth Syst. Sci.* **2018**, *22*, 1299–1315, doi:10.5194/hess-22-1299-2018.

18. Busari, I.O.; Demirel, M.C.; Newton, A. Effect of Using Multi-Year Land Use Land Cover and Monthly LAI Inputs on the Calibration of a Distributed Hydrologic Model. *Water* **2021**, *13*, 1538, doi:10.3390/w13111538.

19. Tikkanen, A. Main River Available online: https//www.britannica.com/place/Main-River.

20. Jung, I.W.; Chang, H.; Risley, J. Effects of Runoff Sensitivity and Catchment Characteristics on Regional Actual Evapotranspiration Trends in the Conterminous US. *Environ. Res. Lett.* **2013**, *8*, 044002, doi:10.1088/1748-9326/8/4/044002.

21. Paradiso, R.; de Visser, P.H.B.; Arena, C.; Marcelis, L.F.M. Light Response of Photosynthesis and Stomatal Conductance of Rose Leaves in the Canopy Profile: The Effect of Lighting on the Adaxial and the Abaxial Sides. *Funct. Plant Biol.* **2020**, *47*, 639, doi:10.1071/FP19352.

22. Samaniego, L.; Kumar, R.; Attinger, S. Multiscale Parameter Regionalization of a Grid-Based Hydrologic Model at the Mesoscale. *Water Resour. Res.* **2010**, *46*, doi:10.1029/2008WR007327.

23. Koch, J.; Demirel, M.C.; Stisen, S. Climate Normalized Spatial Patterns of Evapotranspiration Enhance the Calibration of a Hydrological Model. *Remote Sens.* **2022**, *14*, 315, doi:10.3390/rs14020315.

24. Cornes, R.C.; van der Schrier, G.; van den Besselaar, E.J.M.; Jones, P.D. An Ensemble Version of the E-OBS Temperature and Precipitation Data Sets. *J. Geophys. Res. Atmos.* **2018**, *123*, 9391–9409, doi:10.1029/2017JD028200.

25. Myneni, R., Knyazikhin, Y., Park, T. MCD15A2H MODIS/Terra+Aqua Leaf Area Index/FPAR 8-Day L4 Global 500m SIN Grid V006 [Data Set]. NASA EOSDIS Land Processes DAAC. Accessed 2022-12-18. **2015**, doi:https://doi.org/10.5067/MODIS/MCD15A2H.006.

26. Running, S., Mu, Q., Zhao, M. MOD16A2 MODIS/Terra Net Evapotranspiration 8-Day L4 Global 500m SIN Grid V006 [Data Set]. NASA EOSDIS Land Processes DAAC. Accessed 2022-12-18. **2017**, doi:https://doi.org/10.5067/MODIS/MOD16A2.006.

27. USGS EROS Archive - Digital Elevation - Shuttle Radar Topography Mission (SRTM). *Earth Resour. Obs. Sci. Cent.* **2018**, doi:10.5066/F7K072R7.

28. Panagos, P.; Van Liedekerke, M.; Borrelli, P.; Köninger, J.; Ballabio, C.; Orgiazzi, A.; Lugato, E.; Liakos, L.; Hervas, J.; Jones, A.; et al. European Soil Data Centre 2.0: Soil Data and Knowledge in Support of the <scp>EU</Scp> Policies. *Eur. J. Soil Sci.* **2022**, *73*, doi:10.1111/ejss.13315.

29. *Harmonized World Soil Database (Version 1.2)*; 2012;

30. E-OBS Gridded Dataset.

31. NASA EOSDIS Land Processes Distributed Active Archive Center (LP DAAC) at the USGS Earth Resources Observation and Science (EROS) Center Available online: https://lpdaac.usgs.gov/data/.

32. GRDC Da-ta Available online: https://www.bafg.de/GRDC/EN/02_srvcs/21_tmsrs/210_prtl/prtl_node.html.

33. Hiederer, R. *Mapping Soil Properties for Europe - Spatial Representation of Soil Database Attributes. EUR26082EN Scientific and Technical Research Series*; 2013; ISBN 9789279325168.

34. Liu, Z.; Wei, S.; Li, M.; Zhang, Q.; Zong, R.; Li, Q. Response of Water Radiation Utilization of Summer Maize to Planting Density and Genotypes in the North China Plain. **2023**.

35. Doumit, J.; Sakr, S. Toward a Snow Melt Prediction Map of Mount Lebanon. *InterCarto. InterGIS* **2019**, *25*, 16–27, doi:10.35595/2414-9179-2019-2-25-16-27.

36. Gupta, H. V.; Kling, H.; Yilmaz, K.K.; Martinez, G.F. Decomposition of the Mean Squared Error and NSE Performance Criteria: Implications for Improving Hydrological Modelling. *J. Hydrol.* **2009**, *377*, 80–91, doi:10.1016/j.jhydrol.2009.08.003.

37. Koch, J.; Demirel, M.C.; Stisen, S. The SPAtial EFficiency Metric (SPAEF): Multiple-Component Evaluation of Spatial Patterns for Optimization of Hydrological Models. *Geosci. Model Dev.* **2018**, *11*, 1873–1886, doi:10.5194/gmd-11-1873-2018.

38. Demirel, M.C.; Koch, J.; Rakovec, O.; Kumar, R.; Mai, J.; Müller, S.; Thober, S.; Samaniego, L.; Stisen, S. Impacts of Multi-Basin and Spatial Pattern Calibration on Robustness and Transferability of Hyrologic Model Parameters in Ungauged Basins. **2022**.

39. Demirci, U.; Demirel, M.C. PET Scaling Method with LAI and Aspect in MHM 2022.

40. White, J.T.; Hunt, R.J.; Fienen, M.N.; Doherty, J.E. *Approaches to Highly Parameterized Inversion: PEST++ Version 5, a Software Suite for Parameter Estimation, Uncertainty Analysis, Management Optimization and Sensitivity Analysis*; Reston, VA, 2020;

41. Alp, H.; Demirel, M.C.; Aşıkoğlu, Ö.L. Effect of Model Structure and Calibration Algorithm on Discharge Simulation in the Acısu Basin, Turkey. *Climate* **2022**, *10*, 196, doi:10.3390/cli10120196.